J. Astron. Space Sci. 26(1), 59–74 (2009)

Autonomous Real-time Relative Navigation for Formation Flying Satellites

Sunhwa Shim, Sang-Young Park†, and Kyu-Hong Choi
Astrodynamics and Control Lab, Department of Astronomy, Yonsei University, Seoul 120-749, Korea
email: spark@galaxy.yonsei.ac.kr

(Received February 3, 2009; Accepted February 12, 2009)

Abstract

Relative navigation system is presented using GPS measurements from a single-channel global positioning system (GPS) simulator. The objective of this study is to provide the real-time inter-satellite relative positions as well as absolute positions for two formation flying satellites in low earth orbit. To improve the navigation performance, the absolute states are estimated using ion-free GRAPHIC (group and phase ionospheric correction) pseudo-ranges and the relative states are determined using double-differential carrier-phase data and singled-differential C/A code data based on the extended Kalman filter and the unscented Kalman filter. Furthermore, pseudo-relative dynamic model and modified relative measurement model are developed. This modified EKF method prevents non-linearity of the measurement model from degrading precision by applying linearization about absolute navigation solutions not about the priori estimates. The LAMBDA method also has been used to improve the relative navigation performance by fixing ambiguities to integers for precise relative navigation. The software-based simulation has been performed and the steady state accuracies of 1 m and 6 mm (1σ of 3-dimensional difference errors) are achieved for the absolute and relative navigation using EKF for a short baseline leader/follower formation. In addition, the navigation performances are compared for the EKF and the UKF for 10 hours simulation, and relative position errors are mm-level for the two filters showing the similar trends.

Keywords: relative navigation, GPS, formation flying, extended Kalman filter, unscented Kalman filter

1. Introduction

Satellite Formation Flying has been proposed recently for advanced space missions. Compared to a large individual spacecraft, the formation flying technique provides improved flexibility and redundancy as well as economical efficiency. Also, satellite formations in low Earth orbit can offer higher resolution imagery and interferometry by precise determination of the distance between two satellites. One of the good examples of formation flying is the synthetic aperture radar (SAR) interferometry formation of TerraSAR-X and TanDEM-X satellites for generating highly accurate mapping (Moreira et al. 2004). The mission objective is based on along-track interferometry as well as new techniques with bi-static SAR, and a precise interferometric baseline vector can be determined

†corresponding author

with the relative position knowledge of 1 mm for different along-track separations by GFZ (Geo Forschungs Zentrum) (Moreira et al. 2004). The GRACE mission had been also designed for formation flying satellites with a normal baseline of 220km by NASA (National Aeronautics and Space Administration) and DLR (Deutsches Zentrum fuer Luft- and Raumfahrt). The primary objective of the GRACE mission was to map the long- to medium- wavelength spherical harmonic coefficients of the Earth's gravitational field (Tapley et al. 2004). The precise GRACE baseline accuracy was 1 mm for the along-track (Kroes 2006) compared to the K-band ranging (KBR). The two missions make use of dual-frequency GPS measurements; however, the recent Swedish-led micro-satellite mission PRISMA uses only single-frequency GPS measurement for on-board relative navigation. The goal of the PRISMA mission, planning to launch in 2009, is to demonstrate in-flight technology experiments related to autonomous formation flying, homing and rendezvous scenarios (D 'mico et al. 2008).

These formation flying missions are supported by the determination of the relative positions between satellites; therefore the real-time relative navigation plays a key role in formation maintenance and control. The relative states can be estimated with high precisions since we can take the advantage of differential positioning canceling out common errors. To obtain the precise relative position, single-differential GPS (SDGPS) and double-differenced GPS (DDGPS) measurements are used. Also, GRAPHIC (group and phase ionospheric correction) measurement data is provided for the ion-free absolute navigation using only single-frequency GPS measurements. In addition, the GPS-based navigation system can offer the 3-dimensional nature of the measurements as well as can allow real-time processing. Thus, on-board relative navigation system based on the reliable GPS enables to obtain inter-satellites precise relative positions for autonomous formation flying, and therefore, the research in the areas has been developed actively over the past 10 years.

The studies about low-Earth orbit (LEO) DGPS systems have already produced sub-cm-level relative position accuracies in software or hardware-in-the-loop (HWIL) simulations. Binning & Galysh (1997) demonstrated HWIL simulation using dual frequency GPS measurement for a 5 km baseline and achieved a relative positioning accuracy of 6.56 cm (3-dimensional root-mean-square (RMS)). Busse et al. (2002) estimated the relative position to 1 cm for about 1 km baseline and Ebinuma et al. (2001) showed a 5 cm relative position accuracy in closed loop rendezvous of two spacecraft using single-frequency GPS receivers in HWIL simulations. A study of Montenbruck et al. (2002) presented an accuracy of 0.5 m for a 12 km baseline with single-frequency GPS measurements. Also, HWIL simulation was carried out by Leung & Motenbruck (2005). Here, an accuracy of 1 cm for a 12km baseline and an accuracy of 1.5 mm over 2x4 km separations were obtained for the best case. Furthermore, the recent studies by Kroes (2006) and Marji (2008) showed mm-level relative position accuracies for a 1 km baseline with dual-frequency measurements. In particular, Marji (2008) obtained accuracies of 2 mm, 3 mm, and 2 mm in radial, along-track, and cross-track, respectively.

Based on the early works, the present research has focused on the development of a real-time navigation system using the simulated GPS data not observation data obtained by GPS receivers due to its applicability. For precise relative navigation both single-differenced (SD) GPS C/A code and double-differenced (DD) GPS carrier phase measurements are used, and GRAPHIC measurement is employed to get ion-free pseudo-ranges in absolute navigation algorithm. Since the GPS observables have errors like ionospheric delays, the effect of errors should be reduced as accurate as possible to obtain meaningful geometric ranges between GPS satellites and user satellites. Therefore, the accurate measurement modeling in filter algorithm is required for the precise orbit determination. In particular, the relative measurement model is modified to be linearized at each estimated absolute position for the two user satellites, which is different from the traditional EKF method. The tradi-

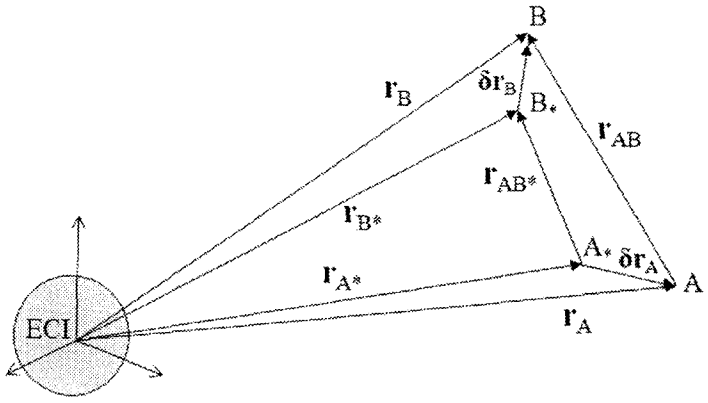

Figure 1. Geometry of GPS satellites and two user satellites (Mohiuddin & Psiaki 2005).

tional measurement equations are linearized at a priori states; the first order approximation can bring about a significant linearization error for highly nonlinear systems. However, the modified method can lead to an accurate estimation for arbitrary baseline applications since the linearization about absolute estimates do not result in significant linearization errors in relative navigation algorithm (Mohiuddin & Psiaki 2005). The reduction of linearization error is a challenging problem in EKF algorithm for large baseline, thus this modified linearization scheme might be a good solution for large baseline applications. Furthermore, the main contribution to this research is to develop the relative navigation algorithm using the UKF as well as the EKF in real-time. The studies about relative navigation using UKF conducted so far has a lot of considerable points to be improved; the work assumed very simple relative dynamics (Lee & Alfriend 2003) and needed so longer simulation time than EKF (Stastny et al. 2008).

Therefore, we will develop and improve the UKF and the EKF relative navigation algorithm providing not only high precision but also appropriate processing time. Following chapters include the measurement and dynamic models and filtering algorithms with ambiguity resolution. Finally, discussion about the simulation results and conclusion for satellite relative navigation are given in the last two sections.

2. Measurement Equations

The navigation filter is comprised of the two steps, time update and measurement update. Before constructing the filter algorithm, the measurement equations are derived and modeled in simple forms based on the simulated GPS measurements for both absolute and relative navigation in this section. The GPS observables generally consist of code pseudo-range, carrier phase pseudo-range, and Doppler data for L1 and L2 frequencies. However, in this study a single-frequency is only used, which is enough for a short baseline relative navigation less than 10 km. Therefore, the possible observables are C/A code pseudo-range, L1 carrier phase, and their combination. First, GRAPHIC data, an arithmetic mean of C/A code and L1 carrier phase, is used for the measurements of absolute

navigation. Using the single-frequency GRAPHIC data can provide the economical efficiency and simplicity of the system due to the advantage of eliminating the dominant measurement error factors, ionosphere errors without dual-frequency GPS measurements (Montenbruck et al. 2006). Here, we assume that the measurement noise for the measurement model of C/A code pseudo-range and L1 carrier phase is Gaussian with the variances, $\sigma^2_{C/A}$ and σ^2_{L1}. As a result, the measurement noise variance for GRAPHIC data is a quarter of the summation of two variances, $\sigma^2_{L1} + \sigma^2_{C/A}$. Also, we assume the measurement noise vectors are not correlated each other, and thus the measurement noise covariance matrix R_* has a diagonal form with the size of J×J where the number of visible satellite is J.

The relative navigation estimate algorithm uses the modified unknowns in order to decompose the relative position solution into a correction to the relative position, which it will determine precisely, and a correction to the absolute position. In Figure 1, the modified relative measurement modeling method is described. The character A and B indicate the true positions of two satellites, the notation AB means the difference B to A, or B-A, and * means the estimated absolute position of the satellites. Here, the state to be estimated is a correction vector $\delta \boldsymbol{r}_{AB}$, which means the correction difference $\delta \boldsymbol{r}_A$ from $\delta \boldsymbol{r}_B$ in Eqs. (1,2); therefore, the relative correction vector enables to estimate the relative position precisely using the absolute estimates.

$$\boldsymbol{r}_A = \boldsymbol{r}_{A^*} + \delta \boldsymbol{r}_A, \quad \boldsymbol{r}_B = \boldsymbol{r}_{B^*} + \delta \boldsymbol{r}_B \tag{1}$$

$$\boldsymbol{r}_{AB} = \boldsymbol{r}_{AB^*} + \delta \boldsymbol{r}_{AB} \tag{2}$$

The code measurement equations for each user satellite are linearized and rearranged to be the known terms on the left and the linear unknown terms on the right (Mohiuddin & Psiaki 2005). Then, the SD code measurement and the DD carrier-phase measurement are modeled for the precise relative navigation. The SD involves two user satellites A and B and one GPS satellites j. We define the new measurement for SD as $\Delta y^j_{P,AB}$ including SD code pseudo-range, and the SD code equations for the two satellites are followed.

$$\Delta y^j_{P,AB} = (\hat{\rho}^j_{AB^*})^T \delta \boldsymbol{r}_A + (\hat{\rho}^j_{B^*})^T \delta \boldsymbol{r}_{AB} + c\delta t_{AB}, \quad j = 1, 2, ..., \mathrm{J} \tag{3}$$

The line of sight vectors of user satellites estimated in absolute navigation algorithm viewed from the GPS satellite are denoted as $\hat{\rho}_{A^*}$ and $\hat{\rho}_{B^*}$, and $\hat{\rho}_{AB^*}$ is a unit vector of the inter-satellite relative position. The SD ionospheric errors are ignored because the user satellite A and B are close, however the SD clock offset δt_{AB} should be considered in the SD measurement equation, Eq. (3). The carrier phase measurement equations are same as the code measurement equations. For the two GPS satellites i and j, the two linearized SD carrier phase equations form the DD carrier phase measurement equation. The new DD measurements $\nabla\Delta y^{ij}_{\phi,AB}$ corresponds the DD carrier phase measurement data in Eq. (4).

$$\nabla\Delta y^{ij}_{\phi,AB} = (\nabla\Delta\hat{\rho}^{ij}_{AB^*})^T \delta \boldsymbol{r}_A + (\nabla\hat{\rho}^{ij}_{B^*})^T \delta \boldsymbol{r}_{AB} + \lambda\nabla\Delta \boldsymbol{a}^{ij}_{AB}, \quad j = 2, 3, ..., \mathrm{J} \tag{4}$$

In this equation, the GPS satellite with the best DOP is selected the first GPS satellite i, and the DD ambiguity term $\lambda\nabla\Delta \boldsymbol{a}^{ij}_{AB}$ is included in the measurement model. The DD carrier phase measurement makes possible to resolve the DD ambiguity vector in Eq. (4) to integer separated from the biases since the initial phases and clock offsets of receivers of two satellites are canceled out, which improves the precision of relative position (Psiaki & Mohiuddin 2007). However, using DD carrier phase measurement could be a problem in case of large baseline formations since the visibility of GPS satellites would be different for each satellite and it will change quickly so that the common visible GPS satellites can be less than the minimum GPS satellite number 4.

Table 1. Dynamics for user satellites (Vallado 2007).

	POD Model	Description
Force Model	Aspherical Earth gravity	70 × 70 JGM3
	Solar and lunar gravity	Astronomical almanac
	Atmospheric drag	Exponential model
	Solar radiation pressure	With eclipse
Reference Frame	Precession & nutation	(Seidelmann 2006)
	Earth rotation & polar motion	UT1 (Seidelmann 2006)
Filtering	EKF and UKF Step	size: 30 sec

We assume that the measurement noise errors show a random behaviors resulting in a normal distribution with expectation value of zero and variances of $\sigma_P^2 I$ and σ_{L1}^2 for code and carrier phase measurements. The mathematical correlation introduced by single differencing yields the measurement noise covariance matrices $R_{\Delta P} = 2\sigma_P^2 I$ and $R_{\Delta\phi} = 2\sigma_{L1}^2 I$. This shows that SD measurements are also uncorrelated. However, the DD measurements are correlated so that the DD carrier phase measurement noise matrix $R_{\nabla\Delta\phi}$ has the off diagonal terms (Hofmann-Wellenhof et al. 2008). Note that the dimension of the unit matrix corresponds to the number of measurements at each time, which is equal to the number of GPS satellites J, and the dimension of the DD measurement noise covariance is J-1. The SD code measurement noise covariance matrix and the DD carrier phase measurement noise covariance matrix are come together in the form of $R = \begin{bmatrix} R_{\Delta P} & 0 \\ 0 & R_{\nabla\Delta\phi} \end{bmatrix}$.

3. Navigation Algorithm

The extended Kalman filter (EKF) has been found to be very robust and adequate for highly precise relative spacecraft positioning. The strength of the filter is that integer ambiguities can be resolved on-the-fly and instantaneously used. In this way the relative position solution directly improves, and the already resolved integer ambiguities automatically aid in the resolution of new ones as they appear over time. The relative spacecraft dynamics of the filter can be handled in an easier way than for the dynamics of batch least-square method (LSQ) since the propagation restarts at every epoch time. Therefore, the EKF algorithm for navigation will be employed allowing autonomous applications for the formation flying satellites, and further, the unscented Kalman filter (UKF) algorithm is also presented and the filter performances are compared with EKF.

The Kalman filter is used to estimate the spacecraft position and velocity vector x_{AB}, clock error T, and ambiguity A in real-time. First, the absolute navigation is performed using each filter and the relative navigation algorithm uses the absolute estimates in measurement modeling. The absolute navigation algorithm is very similar to the relative navigation algorithm; therefore the absolute navigation process can be referred to the algorithm of Shim (2009). In this navigation algorithm, time update involves the propagation of the positions and velocities of two satellites through a numerical integration of the precise dynamic equations by 4^{th} order Rung-Kutta integrator. The 4^{th} order integrator can usually provide for the sufficient precision (Montenbruck & Gill 2001). The perturbations in force model and other filter information used in this study are summarized in Table 1.

3.1 EKF Algorithm for Relative Navigation

The relative navigation algorithm begins by assuming the random process to be estimated can be modeled in the Eq. (5).

$$\dot{x}_{AB} = f(x_{AB}, t) + Dw(t) \tag{5}$$

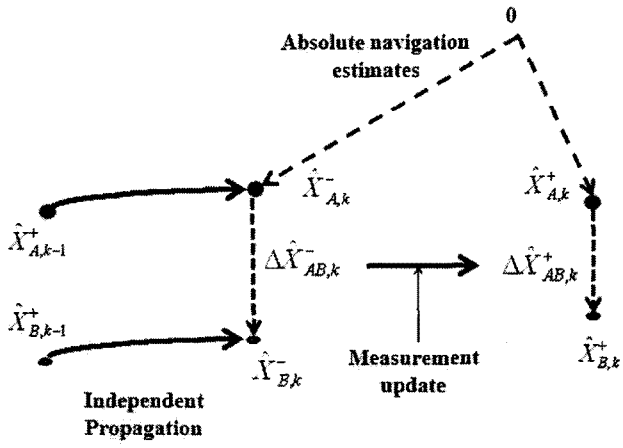

Figure 2. Pseudo-relative dynamic propagation and measurement update.

For relative navigation, the state $x_{AB}(t)$ should contain the absolute position and velocity for the satellites A and the relative position and relative velocity for satellites A and B. Therefore, the relative motion state is defined as $x_{AB}(t) = [r_A(t) \;\; \nu_A(t, r_A) \;\; r_{AB}(t) \;\; \nu_{AB}(T, r_A, r_B)]^T$. The dynamic uncertainties are expressed in the matrix $D = \begin{bmatrix} 0 & I & 0 & 0 \\ 0 & 0 & 0 & I \end{bmatrix}^T_{12\times 12}$ and the process noise vector $w = [w_A \;\; w_B]^T$. We assume the process noise vector is Gaussian. Finally, the filter state for relative navigation involves the correction state $\delta x_{AB} = [\delta r_A \;\; \delta\nu_A \;\; \delta r_{AB} \;\; \delta\nu_{AB}]$ as well as the SD clock offset T_{AB} and the DD ambiguity vector A. Thus the augmented filter state is denoted as $X_{AB} = [\delta x_{AB} \;\; T_{AB} \;\; A]^T$. The satellite motion orbiting with respect to the Earth is described by the dynamic differential equation, which is to add the perturbing accelerations to the two-body equation for each satellite. Therefore, the relative acceleration applied the pseudo-relative dynamic is an only direct difference between accelerations for each satellite, $f(x_{AB}, t) = [\nu_A(t) \;\; a_A(t, r_A, \nu_A) \;\; \nu_{AB}(t) \;\; a_B(t, r_B, \nu_B) - a_A(t, r_A, \nu_A)]^T$. The relative motion state is propagated considering the perturbations in Table 1, and the SD clock offset and the DD ambiguities are constant in time update step. Therefore, the dynamic equation for the augmented filter state becomes Eq. (6).

$$\dot{X}_{AB} = F(X_{AB}, t) + D'w'(t) \tag{6}$$

where $F(X_{AB}, t) = [f(x_{AB}, t) \;\; 1 \;\; I_{J-1}]^T$, $w' = [w_A \;\; w_{AB} \;\; 0 \;\; 0_{J-1}]^T$,

$$D' = \begin{bmatrix} 0 & I & 0 & 0 & 0 & 0 \\ 0 & 0 & 0 & I & 0 & 0 \\ 0 & 0 & 0 & 0 & 0 & 0 \\ 0 & 0 & 0 & 0 & 0 & 0 \end{bmatrix}^T_{(12+J)\times(12+J)}$$

The filter state vector describing satellite motions has 12-dimension, the SD clock offsets $c\delta t_{AB}$ is scalar, and the DD ambiguity vector has (J-1)-dimension resulting the total number of state to be estimated is 12+J where J is the visible GPS satellite numbers.

In the propagation step, the posteriori estimate is numerically integrated for the individual satel-

lite. For the relative state, there is no accurate dynamic equation that demonstrates relative motions between two satellites. Although Hill's equation can describe the relative motion, some strict assumptions should be satisfied. In other words, the motion of a chief satellite should be circular and a deputy satellite should be very close to a chief satellite. Therefore, we will consider the pseudo-relative dynamics that each state is propagated independently. The relative navigation scheme is shown in the Figure 2 (Leung & Montenbruck 2005). The integrated filter states for satellites A and B are directly differenced, and the state is updated using differential measurements. The covariance update is performed between time update step and measurement update step. Covariance is propagated in time domain using Eq. (7) with the simple form of process noise covariance matrix Q.

$$\dot{P} = AP + PA^T + Q \tag{7}$$

After propagation of the state and the covariance matrix in the filter algorithm, the Kalman gain is calculated in Eq. (8) using the measurement noise covariance obtained in chapter 2.

$$K_k = P_{\bar{k}} H_k^T (H_k P_{\bar{k}} H_k^T + R_k)^{-1} \tag{8}$$

Finally, a posteriori states and the covariance matrix are updated in the EKF algorithm, and the estimated relative states indicate the correction terms with respect to the absolute navigation solutions for each satellite A and B (Brown & Hwang 1997). Therefore, using the relations of Eq. (2) the relative positions and velocities are obtained by adding the estimated correction terms to the absolute navigation solutions.

Furthermore, the estimated ambiguities may be float; therefore, we should fix the float ambiguities to the exact integers in the filter algorithm. We have used the LAMBDA method as an integer ambiguity resolution algorithm referred from the Mathematical Geodesy and Positioning of the Delft University of Technology (http://www.lr.tudelft.nl/mgp). The LAMBDA method introduced by Teunissen (1995) can provide the accurate integer ambiguity combinations, and by updating the state vectors with fixed integer ambiguities, we can lead to an improvement for the relative navigation performances.

3.2 UKF Algorithm for Relative Navigation

In contrast to the EKF which uses linearization to approximate the mean and covariance matrix after a nonlinear transformation, UKF uses a set of deterministically chose and nonlinearly transformed points to approximate theses quantities (Lee & Alfriend 2003). Therefore, the construction of the UKF algorithm is thought to be simple compared to the EKF algorithm since the linearization of dynamic and measurement equations in the EKF is very demanding. The UKF algorithm is divided into three main steps: selection of sigma points, propagation of the sigma points, and finally, measurement update of the sigma points (Lee & Alfriend 2003). The propagation and measurement update sequences are similar to the EKF algorithm, thus as the EKF, the nonlinear dynamics for relative navigation is given same as Eq. (6). In addition, the nonlinear measurement models are used in the nonlinear forms as Eq. (9).

$$\begin{bmatrix} \Delta P^j_{C/A,AB} \\ \nabla\Delta L^{j1}_{1,AB} \end{bmatrix} = \begin{bmatrix} (\rho^j_B - \rho^j_A) + c\delta t_{AB} \\ (\Delta\rho^j_{AB} - \Delta\rho^j_{AB}) + \lambda\nabla\delta a^{j1}_{AB} \end{bmatrix} = h(x_{AB}, T_{AB}, A), \quad j = 2, 3, ..., \mathrm{J} \tag{9}$$

The SD code and DD carrier phase measurements $\Delta P^j C/A, AB$ and $\nabla\Delta L^{j1}_{1,AB}$ are represented by the geometric distances of satellite A and B from the j^{th} GPS satellite, ρ^j_A and ρ^j_B, and the relative distance, $\Delta\rho^j_{AB}$. The SD ionospheric error and the SD clock error terms were canceled out

Table 2. Initial osculating orbit parameters.

Orbit Parameters	Satellite A	Satellite B
a (km)	7349.4	7349.4
e	0.039	0.039
i (deg)	98	98
w (deg)	278	278
Ω (deg)	102	102
M (deg)	0	0.008

in Eq. (9). The measurement equations consist of J SD nonlinear equations and J-1 DD nonlinear equations, therefore the 2J-1 measurement equations can be modeled to Eq. (10)

$$\lambda = a^2(N - \kappa) - N \tag{10}$$

In this equation, α, β, and κ are scaling parameters, and the values are $\alpha = 9.5 \times 10^{-4}, \beta = 2$, and $\kappa = 3 - L$ where L is 18 (Lee & Alfriend 2003). In this study, the number of states is J+12 where J is the number of visible GPS satellites. The parameters are determined based on the experiences resulting better performance. The 2N+1 sigma points are then propagated through the nonlinear dynamics and recombined to generate a propagated mean and covariance. The propagated sigma points are updated through the measurement dynamics and also recombined, using the weighting factors, to generate a predicted measurement (Stastny et al. 2008). The measurement noise covariance and the cross correlation matrix are calculated, and the state estimate update and covariance update are obtained using the Kalman gain of Eq. (12) same as the EKF algorithm.

$$K_k = P_k^{xy}(P_k^{yy})^{-1} \tag{11}$$

Here, P_k^{xy} and P_k^{yy} are the cross correlation matrix and the measurement noise covariance. The propagation and measurement update process should be repeated as many as the number of all sigma points, which requires considerable computational time so that we may choose another filter for the complex systems (Lee & Alfriend 2003). However, in this study, the process time for the UKF is not significant factor because the UKF algorithm takes 2.5 times longer than the EKF algorithm. Therefore, the simulation time is enough for the real-time relative navigation applications.

4. Simulation Resutls

To assess the relative navigation algorithm, the simulation is performed in case that two satellites orbiting in the same orbit separated each other with a short baseline. In this leader-follower motion, the distance between two satellites will change as time goes on due to the perturbations and the ecliptic trajectory of its initial orbit although there is no applied force for orbit controls. Therefore, we would like to estimate the baseline vectors from one satellite to another satellite in real-time for the formation maintenance or other applications.

Real world or simulated pseudo-range measurements are required for the navigation system tests in real-time. In this study, we will only deal with the software simulation tests, and the GPS measurement data is provided by the authorized navigation simulator software (STR 6560), SIMGEN. The software SIMGEN can provide the GPS measurements as the real GPS data including some critical measurement errors. The software also allows the option to select the measurement error model depending on the satellite environments; thus, the analysis of error modeling in the navigation algorithm can be possible. We use the simulated GPS measurements including the errors in

pseudo-ranges such as tropospheric errors, ionospheric errors, and small random noise, and other error factors are not considered. A simple SIMGEN scenario has been set to test the real-time relative navigation systems for formation flying satellites. The specifications for the satellites in the scenario were referred to a good test platform PRISMA, the recent formation flying satellite mission, and the simulation is performed for 10 hours after 12:00 April 28, 2008. In the simulation scenario, two satellites are separated 1 km each other in low-Earth orbit with about 900 km altitude. Satellite mass is 150 kg, the drag coefficient is 2.3, cross-section area for drag computation is 0.67 m^2 and the solar radiation pressure coefficient is 1.3, referring to the study by D'mico et al. (2006). We assumed that the shape of two satellites is identical, and the orbit parameters are summarized in Table 2. The number of GPS satellites viewed from the two user satellites is usually more than 7×8 since there is no obstacle to block the GPS signals in space, thus the elevation angle of the user satellite only determines the GPS satellite visibility. Moreover, the two user satellites are located so close that we can assure that the number of visible GPS satellites involved in the relative navigation algorithms is always 6 in this study.

The several cases of simulations for absolute and relative navigation are performed for the EKF and UKF. The navigation accuracies indicating estimation performance mean a standard deviation, 1σ of position errors between true positions and estimated positions of the user satellites. The required accuracies are 1 m for absolute navigation and mm-level in relative navigation in 3-dimension. In following subsections the navigation results are presented for the EKF and UKF and the relative navigation performance of two filters is compared for a short baseline formation.

4.1 Absolute Navigation Results

First, the behaviors of absolute positioning errors using GRAPHIC measurements are illustrated. For precise relative navigation, the absolute positions for each satellite are required in the relative measurement modeling. Therefore, we should find the absolute positions of two satellites ahead of relative positioning. Here, the algorithm test for each satellite has the exact same condition, thus the simulation results of absolute navigation will be presented only for the one satellite, satellite A. The filter state includes position $\boldsymbol{r}_A$, velocity ν_A, and ambiguity $\boldsymbol{a}_A$; initial state errors for each filter algorithm are given by a Gaussian distribution with the standard deviations of 1 km, 1 m/s, and 1 m for initial position, velocity and ambiguity vectors, which are determined as tuning parameters. Also, the process noise covariance and measurement noise covariance are picked up empirically as $Q = diag([0_3 \;\; 10^{-6} \;\; I_3 \;\; 0.25 \;\; 0_6])$ and $R_* = 10^{-6} I_6$ for the EKF algorithm. The UKF algorithm is tested with the same initial state errors and process noise covariance matrix as the EKF and measurement noise covariance matrix is given by $R_* = 10^{-7} I_6$.

The navigation results are expressed in the position errors in meter as simulation time. In Figure 3, the simulation results showed a 3-dimensional accuracy of 0.973 m for the EKF. At 1500 sec and 2800 sec, the position errors are slightly increased, however, overall absolute positions are well estimated with the position errors of zero means and standard deviations of 0.650 m, 0.634 m, and 0.349 m in radial, transverse, and orbit normal direction, respectively. The accuracies are better than the results of the studies of Leung & Montenbruck (2005), 2.5 m in 3-dimensional accuracy. The 3-dimensional position error for the UKF is about 0.967 m, and the standard deviations of errors are 0.474 m, 0.666 m, and 0.516 m for each direction. Compared with the result of EKF, we can deduce that the performance of absolute navigation is very similar for the EKF and UKF. The absolute positions for two filters are well estimated using GRAPHIC measurements with 1 m-level accuracies. Errors for each direction are bounded for all the simulation time, and therefore we can apply the absolute navigation solutions to the relative navigation algorithm for measurement modeling.

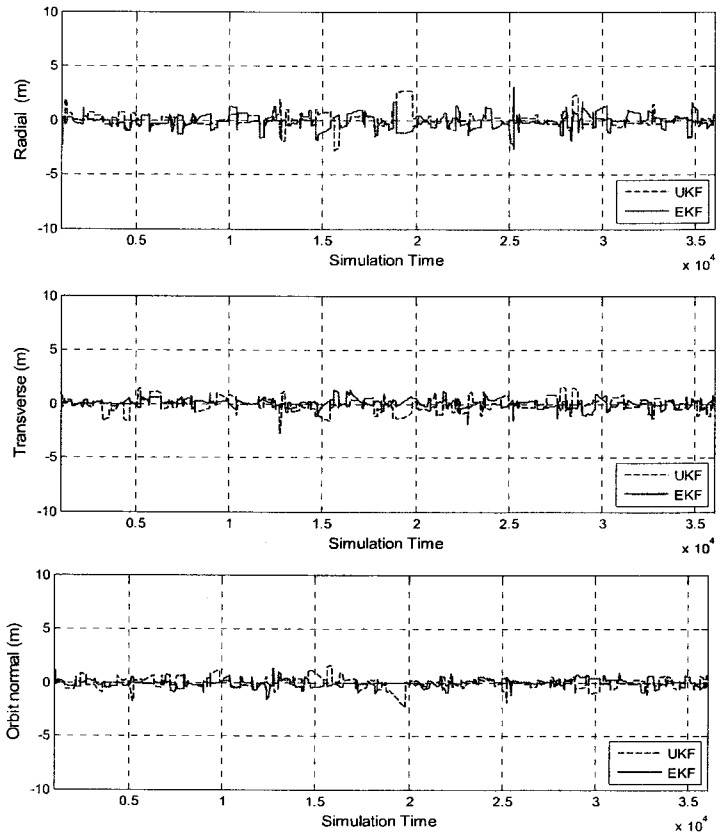

Figure 3. Estimated absolute position errors using EKF and UKF.

Table 3. Initial covariance matrix components for EKF.

State	Case 1	Case 2	Case 3
r_A (km)	1	1	10
ν_A (m/s)	1	1	10
Δr_{AB} (m)	1	10	10
$\Delta \nu_{AB}$ (m/s)	0.1	1	1
A (m)	0.05	1	5

4.2 Relative Navigation Results for EKF

The results of relative navigation using the EKF are provided in this section. For the best performance, the values of process noise covariance and measurement noise covariance are determined empirically as $Q = ([0_3 \;\; 10^{-13} \;\; I_3 \;\; 0_3 10^{-15} \;\; 0.0025 \;\; 10^{-2} I_5])$ and $R = \begin{bmatrix} R_{\Delta P} & 0 \\ 0 & R_{\nabla \Delta \phi} \end{bmatrix}$ where $R_{\Delta P} = 2 \times 10^{-8} I_6$ and $R_{\nabla \Delta \phi} = 10^{-9} \times (I_5 + I_5)$.

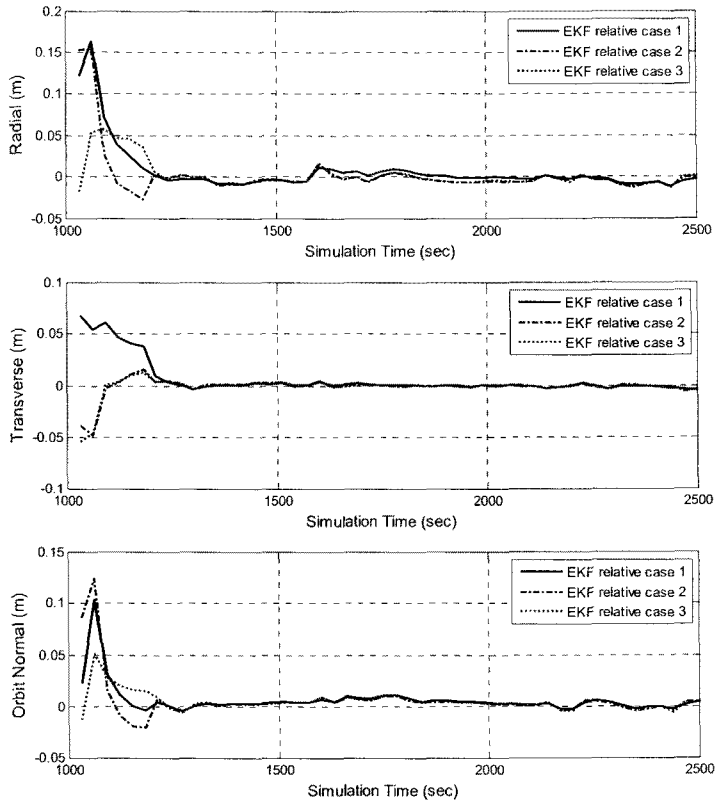

Figure 4. Estimated relative position errors for EKF depending on the initial covariance matrix P.

Table 4. Estimated relative position errors for EKF depending on the initial covariance matrix P.

	Case 1	Case 2	Case 3
3-D (mm)	6.39	7.37	7.76
Radial (mm)	4.08	4.80	4.85
Transverse (mm)	4.09	4.64	5.09
Orbit normal (mm)	2.71	3.12	3.28

In this matrix form, the notation I_5 indicates the 5 by 5 square matrix in which all components are 1. The Figure 4 illustrates the behaviors of the error of the relative navigation. Relative position errors for case 1 are converged instantly and a steady-state accuracy of 6.39 mm is achieved. Accuracies of each component are 4.08 mm, 4.09 mm, and 2.71 mm in radial, transverse, and orbit normal direction, respectively. The values are sufficiently accurate for autonomous formation flying applications.

Depending on the initial error covariance matrices, the filter algorithm can lead to different nav-

Table 5. Initial covariance matrix components for UKF.

State	Case 1	Case 2	Case 3
r_A (km)	1	1	1
ν_A (m/s)	1	1	1
Δr_{AB} (m)	1	1	10
$\Delta \nu_{AB}$ (m/s)	0.1	0.1	1
A (m)	0.05	0.5	5

Table 6. Estimated relative position errors for UKF depending on the initial covariance matrix P.

	Case 1	Case 2	Case 3
3-D (mm)	7.25	11.6	10.9
Radial (mm)	4.18	7.44	6.38
Transverse (mm)	4.59	7.23	7.10
Orbit normal (mm)	3.74	5.29	5.24

igation performances. Here, the initial error covariance means the values of initial state errors. Thus, we will compare the filter performances for several cases of different initial state errors. The filter states consist of position r_A, velocity ν_a, relative position Δr_{AB}, relative velocity $\Delta \nu_{AB}$, and double-differential ambiguity vector A. Each component of the initial state errors is summarized in Table 3 for 3 cases. The case 1 in Table 3 is corresponding to the best performance case and the cases of large initial state errors are given by the case 2 and case 3 in Figure 4. The 3-dimensional accuracies of relative positions are 6.39 mm, 7.37 mm, and 7.76 mm for case 1, case 2, and case3, respectively and the standard deviations of the position errors for each direction are summarized in Table 4. These accuracies are almost the same level, and the steady state relative position errors have similar trends in Figure 4. Furthermore, the ambiguity states including initial errors will be determined to the correct integer values soon, and the estimation errors can converge into zero mean within a few steps since we only deal with the relative navigation algorithm of a short baseline formation. Therefore, we can conclude that the appropriate initial state errors can assure an affordable performance for relative navigation.

4.3 Relative Navigation Results for UKF

The relative navigation performance using UKF is presented and compared with the EKF results. The several cases of the different initial covariance matrices are tested using the values in Table 5. The UKF relative position accuracies with respect to the initial covariance matrix are represented in Table 6, and the position error performances for 3 cases of initial covariance matrices are shown in Figure 5. The relative position errors of the case 1 have the initial peaks of ± 0.1 m and the errors converge to zero mean rapidly. The position errors in all directions show good performances and the standard deviations for each direction are 4.18 mm, 4.59 mm, and 3.74 mm for radial, transverse, and orbit normal direction. Therefore, we can conclude that the magnitudes of position errors are compatible for the EKF results. For the case 2 and case 3, the estimation errors have the similar trend in all directions, however, the initial oscillations for transverse and orbit normal directions are relatively large compared to the case 1. The 3-dimensional difference accuracies for case 2 and case 3 are 11.6 mm and 10.9 mm, which is larger than the required accuracy i.e., mm-level. This indicates that the EKF algorithm performance is better than the UKF performance

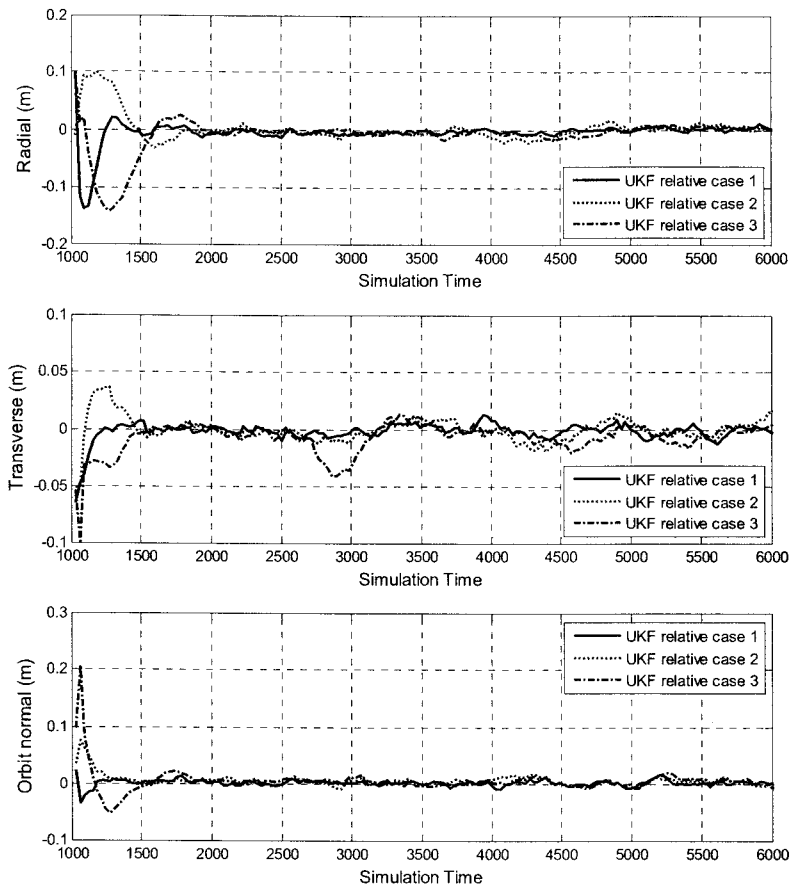

Figure 5. Estimated relative position errors for UKF depending on the initial covariance matrix P.

when the initial covariance is large. In general, however, the initial covariance for each filter is not applied in the same way; rather the tuning parameters like initial covariance matrices are selected independently for the best performance case. The UKF noise covariance for the best case is given by $Q = diag([0_3 10^{-11} \;\; I_3 \;\; 0_3 10^{-13} \;\; I_3 \;\; 0.0025 \;\; 10^{-2} I_5])$ and $R = \begin{bmatrix} R_{\Delta P} & 0 \\ 0 & R_{\nabla\Delta\phi} \end{bmatrix}$ where $R_{\Delta P} = 2 \times 10^{-9} I_6$ and $R_{\nabla\Delta\phi} = 10^{-11} \times (I_5 + I_5)$.

4.4 Comparison of Relative Navigation Performance between EKF and UKF

The relative navigation performance for the EKF and UKF is compared for the same order of initial state errors in Figure 6. For a short baseline, the same initial state errors of 1 km, 1 m/s, 1 m, 10 cm/s, and 0.05 m are used for two filters, and it is expected to have similar performance. The dynamic equations and measurement equations are the same, and the measurement noise and process noise covariance matrices have only different values depending on the filter type. In Figure 6, the position errors for the two filters show the similar trends. Although the initial position

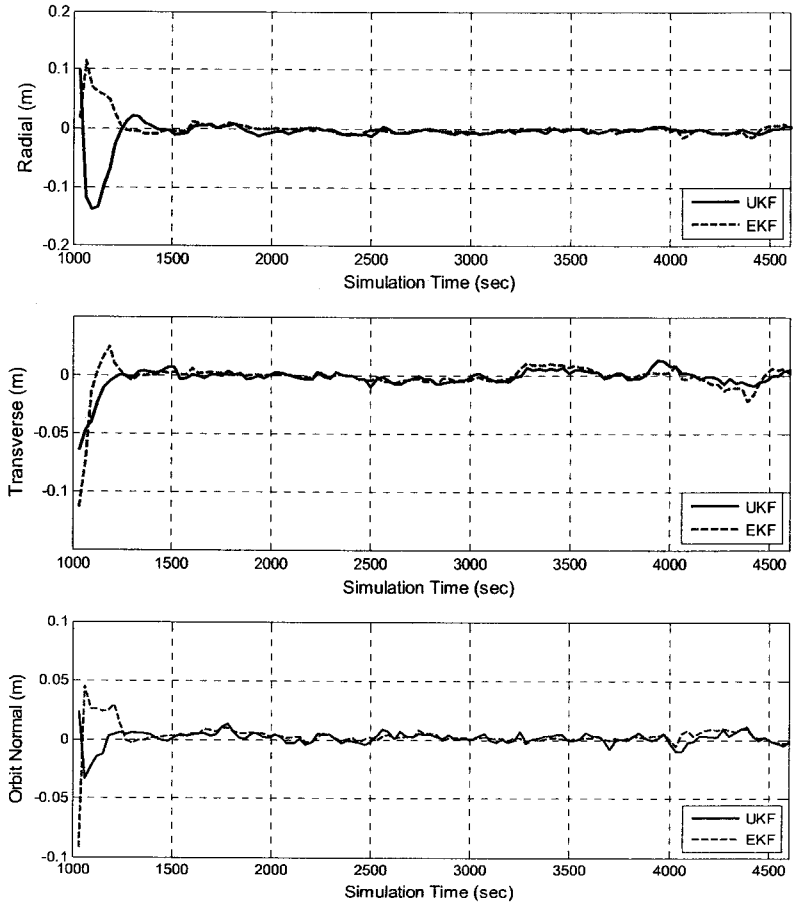

Figure 6. EKF and UKF performance comparison.

error is different in each direction, the steady state relative position errors become almost same after 2,000 sec from the simulation start. Better performances can be expected for the UKF since the linearization approximations are not applied; however, the overall relative navigation performances are nearly same for the two filters. This is because that the EKF algorithm has become less sensitive to the linearization errors of the measurement equations by using the modified measurement model and the initial baseline of two satellites in formation is relatively short. If a distance for the formation flying satellites is longer than 10 km, then the linearization errors for the dynamic model and measurement model of EKF may be significant.

5. Conclusions

The primary objective of this study is to develop the navigation algorithm and validate the estimated relative navigation performances in real-time for autonomous formation flying using single-

frequency GPS measurements. For the main contribution for this study, we have been developed the UKF algorithm as well as the EKF for relative navigation. Several cases of simulations are performed, and finally, the steady-state 3-dimensional relative position accuracies of mm-level have been achieved for the two filters using the simulated GPS measurements.

The 3-dimensional absolute and relative position accuracies over 1 km baseline in LEO satellite are about 0.973 m and 6.39 mm for the EKF and 0.967 m and 7.25 mm for the UKF. Therefore, the aimed overall relative navigation accuracy of sub-cm has been achieved for the EKF and the UKF algorithms and ambiguity resolution is successful in real-time using LABDA method. The relative navigation performances of two filters have shown the similar trends, and the 3-dimensional accuracies are same order. Also, it takes 2.5 times longer for the UKF algorithm to be simulated than the EKF algorithm. Although the UKF algorithm requires longer simulation time than the EKF, the real-time processing of the UKF is allowed for the satellite relative navigation. From the earlier results, therefore, it is concluded that this study can provide the relative position accuracy enough for autonomous formation flying missions and might be a basis for further scientific applications such as high resolution interferometry and autonomous rendezvous.

Acknowledgements: This work was supported by the Korea Science and Engineering Foundation (KOSEF) through the National Research Laboratory Program funded by the Ministry of Science and Technology (No. M10600000282-06J0000-28210).

References

Binning, P. W. & Galysh, I. 1997, in ION GPS, ed. H. L. Kite-Powell (Santa Monica: ION), p.407

Brown, R. G. & Hwang, P. Y. C. 1997, Introduction to Random Signals and Applied Kalman Filtering (New York: Wiley & Sons, Inc.), p.214

Busse, F. D., How, J. P., & Simpson, J. 2002, in ION GPS (Oregon: ION), p.2047

D'mico, S., Gill, E., Garcia, M., & Montenbruck, O. 2006, in Satellite Navigation User Equipment Technology, Navitec 2006 (Noordwijk: Satellite Navigation User Equipment Technology)

D'mico, S., Montenbruck, O., Larsson, R., & Chasset, C. 2008, in AIAA Guidance, Navigation and Control Conference (Hawaii: AIAA), p.6661

Ebinuma, T., Bishop, R. H., & Lightsey, E. G. 2001, in ION GPS (Salt Lake City: ION), p.2286

Hofmann-Wellenhof, B., Lichtenegger, H., & Wasle, E. 2008, GNSS, ed. B. Hofmann-Wellenhof (Austria: Springer-Verlage Wien), p.105

Kroes, R. 2006, PhD Dissertation, Delft University of Technology

Lee, D. -J. & Alfriend, K. T. 2003, in AAS/AIAA Astrodynamics Specialist Conference (Big Sky: AIAA) p.230

Leung, S. & Montenbruck, O. 2005, JGCD, 28, 2

Marji, Q. 2008, PhD Dissertation, The University of Calgary

Mohiuddin, S. & Psiaki, M. L. 2005, in AAIA Guidance, Navigation, and Control Conference (San Francisco: AIAA), p.6054

Montenbruck, O., Ebinuma, T., Lightsey, E. G., & Leung, S. 2002, Aerospace, Science and technology, 6, 435

Montenbruck, O. & Gill, E. 2001, Aerospace, Science and technology, 5, 209

Montenbruck, O., Gill, E., & Markgraf, M. 2006, in Satellite Navigation User Equipment Technology, Navitec 2006 (Noordwijk: Satellite Navigation User Equipment Technology)

Moreira, A., Krieger, G., Hajnsek, I., Hounam, D., & Werner, M. 2004, IEEE, 2, 1000

Psiaki, M. L. & Mohiuddin, S. 2007, JGCD, 30, 6

Seidelmann, P. K. 2006, Explanatory Supplement to the Astronomical Almanac, ed. P. K. Seidelmann (Sausalito: Univ, Science Books), p.103

Shim, S. 2009, Msc Thesis, Yonsei University

Stastny, N. B., Bettinger, R. A., & Chavez, F. R. 2008, in AIAA/AAS Astrodynamics Specialist Conference (Hawaii: AIAA), p.6661

Tapley, B. D., Bettadpur, S., Ries, J. C., Thompson, P. F., & Watkins, M. 2004, Science, 305, 5683

Teunissen, P. J. G. 1995, Journal of Geodesy, 70, 65

Vallado, D. A. 2007, Fundamentals of Astrodynamics and Applications, 3rd ed., ed. J. R. Wertz (Hwthorne: Microcosm Press), p.536